Unamplified Coherent Transmission of Net 500 Gbps/Polarization/λ for Intra-Datacenter Interconnects

Essam Berikaa, *Graduate Student Member, IEEE*, Md Samiul Alam, *Graduate Student Member, IEEE*, and David V. Plant, *Fellow, IEEE*

***Abstract*— To keep up with the growing data traffic demand, spectrally efficient coherent systems are envisioned to replace intensity modulation direct detection (IMDD) systems in short-reach intra-datacenter interconnects (DCI). In this work, we characterize and test an unamplified coherent transmission system employing a C-band thin-film lithium niobate (TFLN) in-phase quadrature modulator (IQM) that has 65 GHz 6-dB electro-optic bandwidth and 1.25 V half-wave voltage (V_π). We demonstrate the transmission of 128 (124) Gbaud 32QAM over 2 (10) km on a single polarization with 2.5 V_{pp} drive signals below the 20% overhead (OH) soft-decision forward error correction (SD-FEC) BER threshold of 2.4×10^{-2}, corresponding to a net rate of 533 (516) Gbps. We evaluate and discuss the digital signal processing (DSP) requirements. Our results and analysis show the potential of shifting to coherent systems for high-capacity short-reach links below 10 km.**

***Index Terms*— Optical interconnects, coherent communication, thin-film lithium niobate, intra-datacenter interconnects.**

I. Introduction

THE growing deployment of cloud-based services, augmented reality applications, and high-definition streaming platforms is driving an exponential increase in data traffic, which mandates a proportional growth in the intra-DC and DCI transport capacities [1]. Although IMDD systems are standardized for short-reach applications ($<$ 10 km) at 200 Gbps/λ [2], their capacity is stretched to its limits. Looking ahead, the available devices' performance alludes that IMDD systems cannot support 400G/λ for DCI reach. To date, there have been few demonstrations of IMDD systems operating at net 300-350 Gbps/λ [3], [4], [5], [6], [7]. However, achieving higher capacities requires employing a higher PAM order than PAM8 or operating at symbol rates beyond 140 Gbaud, which is very challenging with the existing RF components and electro-optic modulators [8]. Therefore, a paradigm shift towards coherent systems for high-speed short-reach links is envisioned [9], [10], [11]. Coherent systems achieve higher data rate capacities because of their higher spectral efficiency at the same symbol rates, which comes at the expense of added DSP complexity and hardware overhead. The developments in ASIC design and fabrication ease the inclusion of the extra DSP blocks of coherent systems. Considering the 7 and 5 nm technology nodes, the ASIC power consumption of coherent and IMDD systems are comparable for short-reach applications ($<$ 2km) with negligible difference at 5 nm [12]. Besides, a comparison between 400G coherent transceivers and 4λ 400G IMDD transceivers in the intra-datacenter reach showed that coherent transceiver modules achieve a higher optical power budget (achievable optical path loss) at similar ASIC power consumption [13]. Therefore, the specifications of next-generation short-reach coherent transceivers are being studied to ensure that the power envelope is competitive versus IMDD solutions [11]. Although coherent receivers offer higher detection sensitivity because of the mixing of the signal with local oscillator (LO), operating without optical amplification mandates reducing the link overall optical loss. A low loss electro-optic modulator with a low V_π (for low modulation loss) is necessary to maintain the optical power at detectable levels even in the absence of trans-impedance amplifiers (TIAs), as in this work. High bandwidth electro-optic modulators exist on different material systems, including lithium niobate (LiNbO3), gallium arsenide (GaAs), indium phosphide (InP), and silicon (Si). However, thin-film lithium niobate (TFLN) modulators stand as a promising candidate for unamplified coherent systems because of their very low optical propagation loss ($<$ 0.7 dB/cm), enabling long devices with low V_π, while maintaining high bandwidths due to the low RF loss [14], [15].

This work evaluates the transmission performance of a C-band unamplified coherent system employing a high bandwidth TFLN IQM and TIA-free PIN photodiodes over short distances (2 to 10 km). We analyze the driving voltage and DSP requirements for optimum performance. We experimentally demonstrate the transmission of 124 Gbaud 32QAM on a single polarization over 10 km of standard single-mode fiber (SSMF) with 2.5 V_{pp} drive signals below the 2.4×10^{-2} SD-FEC BER threshold, corresponding to a net rate of 516 Gbps. Moreover, we transmit 124 Gbaud 16QAM over 10 km below the 3.8×10^{-3} hard-decision (HD)-FEC BER threshold, which corresponds to 465 Gbps net rate and is aligned with the envisioned 800G LR1 standard [16]. Our results support the promise of practical unamplified coherent systems with data rates beyond 1 Tbps/λ over the intra-DCI reach with standard polarization division multiplexing and currently available electronics analog bandwidths.

Manuscript received 12 July 2022; revised 16 August 2022; accepted 1 September 2022. Date of publication 5 September 2022; date of current version 16 September 2022. *(Corresponding author: Essam Berikaa.)*

The authors are with the Photonic Systems Group, Department of Electrical and Computer Engineering, McGill University, Montréal, QC H3A 0E9, Canada (e-mail: essam.berikaa@mail.mcgill.ca; md.samiul.alam@mail.mcgill.ca; david.plant@mcgill.ca).

Color versions of one or more figures in this letter are available at https://doi.org/10.1109/LPT.2022.3204178.

Digital Object Identifier 10.1109/LPT.2022.3204178

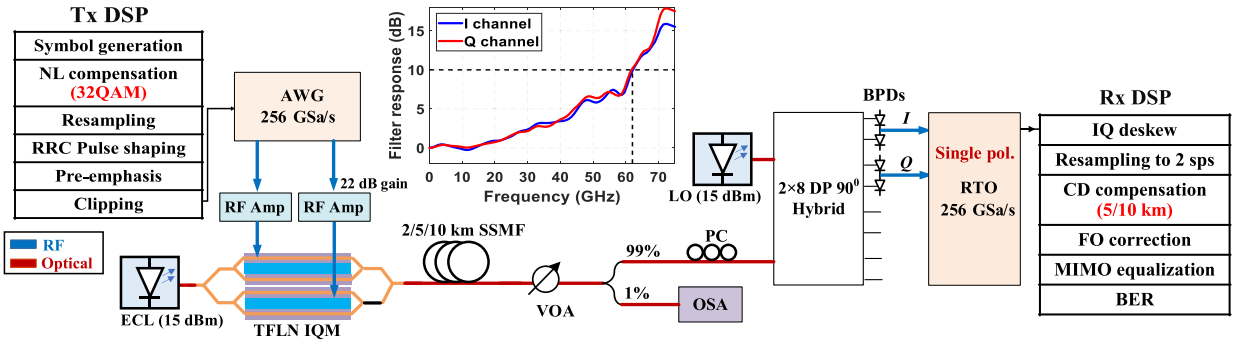

Fig. 1. The experimental setup and DSP blocks applied at the transmitter (Tx) and receiver (Rx). The inset shows the pre-compensation filters response.

II. IQM Characterization and Experimental Setup

The experimental setup and DSP routines employed in this work are presented in Fig. 1. The structure follows the conventional coherent transmission systems architecture. At the transmitter, we generate the QAM symbols from a random binary sequence. Due to the higher number of levels and sensitivity to non-linearity, we apply non-linear pre-distortion (NLPD) on the 32QAM symbols using a 3-symbol non-linear lookup table (NLLUT) [17]. The complex signal is up-sampled and shaped with a root-raised cosine (RRC) filter. Then, the In-phase (real) and quadrature (imaginary) components of the signal are filtered with the pre-compensation filters depicted in the inset of Fig. 1. These digital filters pre-compensate the frequency response of the arbitrary waveform generator (AWG) channel and the RF amplifier up to 70 GHz. The 10 dB point is around 60 GHz; thus, the RRC filter roll-off factor (α) is set to limit the signal bandwidth to 60 GHz for symbol rates under 120 Gbaud. The I and Q signals are clipped to limit their peak-to-average power ratio (PAPR) before loading the signals to the AWG running at 256 GSa/s. The observed optimum PAPR of the digital signal is ~9 dB. The AWG output is amplified using a matched pair of 60 GHz 22-dB gain RF amplifiers (SHF804b), which drives the TFLN IQM using a GSG-GSG 67 GHz RF probe, as shown in the inset of Fig. 2(a). The IQM is optically connected through vertical grating couplers that have peak transmission around 1563 nm and back-to-back insertion loss of 11 dB (5.5 dB/facet). This work uses external cavity lasers with 100 kHz linewidth and 15 dBm optical power. The output of the IQM is transmitted over different lengths of SSMF and followed by a variable optical attenuator (VOA) for sweeping the received optical power (ROP), which is the input optical power to the coherent receiver (hybrid). The receiver employs a 2×8 dual-polarization (DP) optical hybrid that mixes the signal with the local oscillator (LO). Therefore, only 12 dBm of the LO power is actively coupled to our single-polarization signal and a polarization controller (PC) is used to align the signal polarization state with the LO. The hybrid outputs are detected by a pair of 70 GHz balanced photodiodes (BPD) and digitalized by the 256 GSa/s real-time oscilloscope (RTO). The offline receiver DSP deskew the received signals as the employed BPDs are not matched, then Gram-Schmidt orthogonalization compensates for the hybrid imperfections and the fixed impairments of the system. The signals are resampled to 2 samples per symbol (sps) for chromatic dispersion (CD) compensation and frequency offset (FO) correction. Then, a 51-tap T/2-spaced 2×2 multiple-input-multiple-output (MIMO) equalizer with real-valued coefficients and interleaved with a second-order phase-locked loop (PLL) is employed to track the phase noise and compensate for the frequency response of the RF probes, IQM, and BPDs. The real-valued MIMO equalizer filters each quadrature independently and can correct the power imbalance and timing skew between the I and Q quadratures [18]. Finally, the BER is calculated based on the demapped bit sequence of the received symbols.

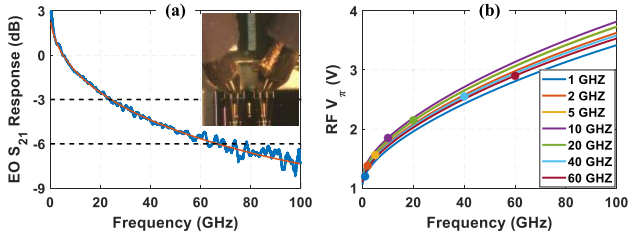

Fig. 2. (a) The frequency response of the TFLN IQM normalized to 5 GHz. (b) The measured and extrapolated RF V_π.

The TFLN IQM is composed of nested MZMs with 23 mm coplanar waveguide electrodes and on-chip termination close to 50 Ω. The bias points are set with thermal phase shifters, to minimum transmission (null) for the children MZMs and to quadrature for the parent MZM. The measured small-signal electro-optic (EO) frequency response (S_{21}) of a MZM identical to those used in the IQM is shown in Fig. 2(a). The characteristic slow roll-off response of TFLN MZMs is observed with a 3-dB bandwidth of 24 GHz and 6-dB bandwidth of 65 GHz. Fig. 2(b) shows the measured RF V_π at different frequencies. Each data point is extrapolated from DC to 100 GHz using the measured EO S_{21} response. The measured low-MHz V_π is 1.25 V that increases to ~3 V at 60 GHz.

III. Transmission Results

The summary of the transmission experiment results is presented in Fig. 3(a). On a single polarization, we transmit 128 (124) Gbaud 16QAM over 2 (10) km under the 6.7% OH HD-FEC BER threshold of 3.8×10^{-3}, which represents a net rate of 480 (465) Gbps. Adopting a higher FEC threshold, we demonstrate the transmission of 128 (124) Gbaud 32QAM over 2 (10) km at a BER below the 2.4×10^{-2} threshold of the 20% OH SD-FEC, corresponding to a net

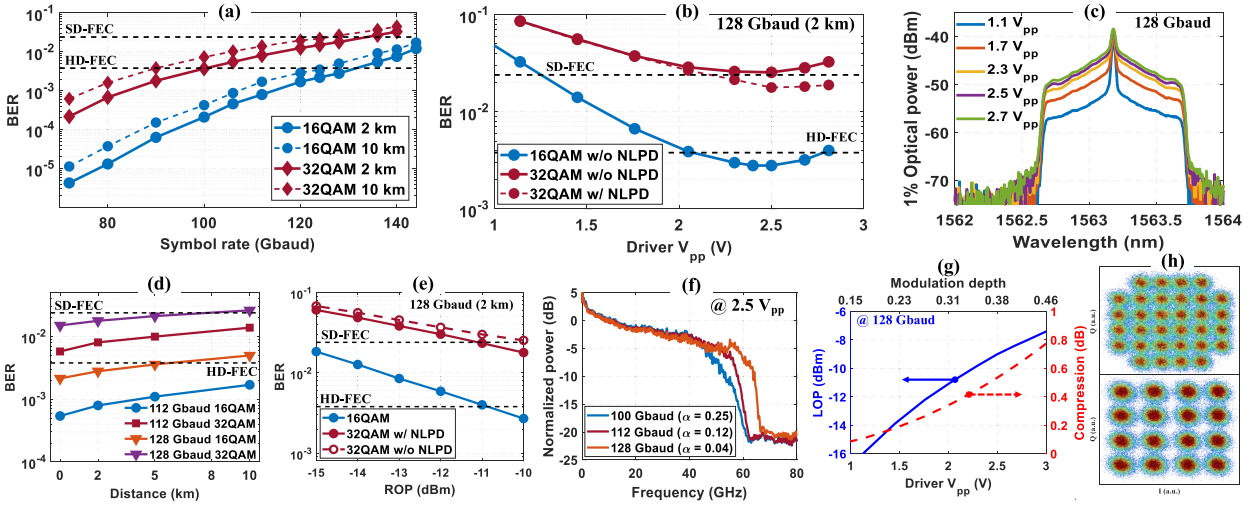

Fig. 3. (a) The BER versus the symbol rate. (b) The BER sensitivity to the drive voltage. (c) The optical spectra of 128 Gbaud 32QAM at different drive voltages at 0.03 nm. (d) The BER versus the transmission distance. (e) The BER versus ROP at 128 Gbaud after 2 km transmission. (f) The received RF spectra at different symbol rates of 32QAM. (g) The measured launch optical power (LOP) into the fiber (solid, blue) and the calculated IQM nonlinear compression (dashed, red) versus the driving voltage with the modulation depth on the top axis. (h) The received constellations of 124 Gbaud 16QAM and 32QAM after 10 km.

rate of 533 (516) Gbps. The BER versus the transmission distance of 112/128 Gbaud 16QAM and 32QAM signals is given in Fig. 3(d). After compensating the CD, the degradation in transmission performance from 2 km to 10 km arises from the ∼1.5 dB extra fiber loss, which reduces the received optical power (ROP) in the absence of optical amplification. Fig. 3(b) shows the BER dependency on the driving voltage for 128 Gbaud signals transmitted over 2 km of SSMF. The observed optimum drive voltage is 2.5 V_{pp}. The non-linearity stemming from the RF amplifier and IQM transfer function dominates the analog-to-digital converter (ADC) noise beyond 2.5 V_{pp}, which degrades the BER performance. Fig. 3(g) shows the output optical power of the IQM launched into the fiber versus the driving voltage and the modulation depth ($M_D = V_{pp}/2V_\pi$), assuming an RF V_π of 3.25 V (64 GHz), besides the calculated non-linear compression arising from only the IQM transfer function ($C_{IQM} = -20\log_{10}(\mathrm{sinc}(\pi M_D/2))$, as defined in [19]. Considering only the IQM non-linear transfer function, the optimum modulation depth is between 0.5 and 0.6, which addresses the tradeoff between modulation loss and non-linear compression [19]. However, the employed RF amplifier 1 dB compression point is 2.5 V_{pp}, which increases the transmitted signal non-linearity and dedicates operating at a lower modulation depth. At 2.5 V_{pp}, the launch optical power (LOP) into the fiber is −9 dBm. The optical spectra of 128 Gbaud 32QAM signals as a function of the drive voltage are shown in Fig. 3(c) at 0.03 nm resolution. The considerable carrier leakage comes from the modest extinction ratio of the child MZMs (∼20 dB). The BER sensitivity to the received optical power (ROP) at 128 Gbaud after 2 km fiber transmission is depicted in Fig. 3(e), the BER degrades rapidly with the ROP as the system is limited by the receiver sensitivity and the ADC noise. Replacing the vertical grating couplers (5.5 dB/facet) with edge couplers (2.5 dB/facet) shall increase the ROP by 6 dB, which will increase the SNR and improve the transmission performance considerably. Considering the 128 Gbaud 32QAM signal, a 1 dB ROP gain is observed at the SD-FEC threshold when NLPD is employed. Although our experimental setup does not include TIAs after the BPDs, it detects signals below −10 dBm owing to mixing with the LO and the higher detection sensitivity of coherent receivers. Fig. 3(f) plots the received RF spectra at different symbol rates. The 128 Gbaud signal experiences ∼7 dB drop at 60 GHz, which corresponds to the combined frequency response of the RF probes, TFLN IQM, and BPDs, and requires large number of MIMO taps for proper equalization. Fig. 3(h) shows the constellations of 124 Gbaud 16QAM and 32QAM after 10 km transmission, which respectively correspond to net rates of 465 and 516 Gbps.

Employing an edge-coupled IQM will save an extra 6 dB of optical power, while a DP IQM will result in a 3 dB reduction in the optical power per polarization; yielding a net 3 dB improvement in the power budget per polarization. This supports the potential of extending our results to dual polarization and realizing net 1 Tbps/λ intra-DCIs.

It is yet debatable whether to employ O-band or C-band lasers in such short-reach unamplified coherent systems. In the O-band, the impact of CD is negligible; however, the fiber loss is slightly higher (0.35 dB/km) compared to the C-band (0.2 dB/km). Moreover, the O-band optical hybrids and BPDs are commercially available, but not as mature as the C-band components. Thus, the primary drawback of operating in the C-band is the need to digitally compensate for the CD, which increases the ASIC power consumption [9], [10]. For 2 km reach, the accumulated CD is adequately low that it does not require a dedicated DSP block for compensation [9], [20]. In this work, we adopted the conventional time-domain finite impulse response (FIR) CD compensation filter [21]. For short-reach applications up to 10 km, compensating the CD in the time domain is advantageous compared to the frequency domain equalization (FED). Because it requires modest number of filter taps (less than 100), which is computationally less exhausting compared to the computation of the fast Fourier transform (FFT). Fig. 4(a) shows the BER sensitivity to the length of the MIMO filters for 128 Gbaud

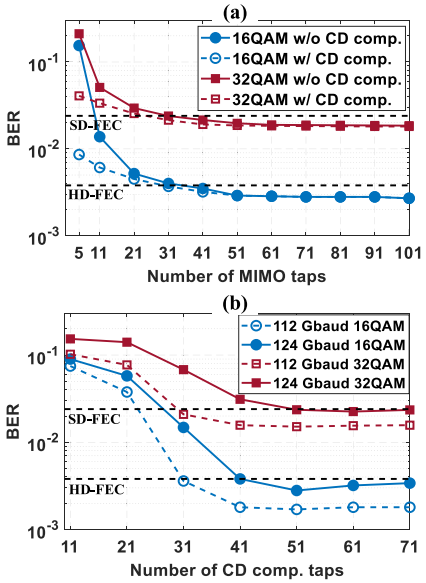

Fig. 4. (a) The BER performance versus the number of MIMO taps for 128 Gbaud signals after 2 km. (b) The BER sensitivity to the CD compensation filter length after 10 km transmission.

signals after 2 km transmission with and without CD compensation. It is observed that 51 taps are sufficient to reach the BER floor. Interestingly, when sufficient MIMO filter taps are employed, the performance with and without CD compensation converge to the same BER. This confirms that up to 2 km (∼34 ps/nm), the MIMO adaptive filtering effectively equalizes the frequency response and compensates for the chromatic dispersion simultaneously; dispensing the need to have a dedicated CD compensation step. Considering 10 km transmission (∼170 ps/nm), Fig. 4(b) shows the BER dependency on the length of the CD compensation FIR filter. The required filter length is independent of the QAM order and is proportional to the square of the symbol rate (B^2); thus, we reach the BER floor for 112 Gbaud signals with 41 taps, while 51 taps are needed for the 124 Gbaud signals. With the advancements in ASIC performance and progression towards smaller technology nodes, the constraints on ASIC power consumption are relaxed and compensating the CD digitally adds modest overhead [12].

IV. Conclusion

In this work, the potential of unamplified coherent transmission systems for short-reach intra-datacenter links (up to 10 km) is studied. Our experimental setup employs the conventional coherent transmission architecture in the C-band with a 65 GHz 6-dB bandwidth, 1.25 V V_π TFLN IQM. On a single polarization with 2.5 V_{pp} drive signals, we transmit 128 (124) Gbaud 32QAM over 2 (10) km under the 20% overhead SD-FEC BER threshold of 2.4×10^{-2}, which corresponds to a net rate of 533 (516) Gbps. Up to 2 km, our analysis reveals that the chromatic dispersion is sufficiently low, and the MIMO equalizer compensates it without requiring a dedicated CD compensation block. For the transmission of 124 Gbaud 32QAM over 10 km, 51 FIR taps are needed to compensate for the CD and minimize the pre-FEC BER. This work shows the potential of unamplified coherent systems for high-speed intra-DC links and campus interconnects with capacities exceeding net 1 Tbps/λ with dual-polarization implementation, and using current electronics capabilities.

Acknowledgment

The authors would like to thank HyperLight for the TFLN modulator.

References

[1] U. Cisco, "Cisco annual internet report (2018–2023) white paper," Cisco, San Jose, CA, USA, White Paper, 2020. [Online]. Available: https://www.cisco.com/c/en/us/solutions/collateral/executive-perspectives/annual-internet-report/white-paper-c11-741490.html

[2] *800G Pluggable MSA*. Accessed: Aug. 14, 2022. [Online]. Available: https://www.800gmsa.com/

[3] N.-P. Diamantopoulos *et al.*, "$>$100-GHz bandwidth directly-modulated lasers and adaptive entropy loading for energy-efficient $>$300-Gbps/λ IM/DD systems," *J. Lightw. Technol.*, vol. 39, no. 3, pp. 771–778, Feb. 1, 2021.

[4] M. S. Alam, X. Li, M. Jacques, E. Berikaa, P.-C. Koh, and D. V. Plant, "Net 300 Gbps/λ transmission over 2 km of SMF with a silicon photonic Mach–Zehnder modulator," *IEEE Photon. Technol. Lett.*, vol. 33, no. 24, pp. 1391–1394, Dec. 15, 2021.

[5] M. S. Bin Hossain *et al.*, "402 Gb/s PAM-8 IM/DD O-Band EML transmission," in *Proc. Eur. Conf. Opt. Commun. (ECOC)*, Sep. 2021, pp. 1–4.

[6] M. S. Alam, E. Berikaa, and D. V. Plant, "Net 350 Gbps/λ IMDD transmission enabled by high bandwidth thin-film lithium niobate MZM," *IEEE Photon. Technol. Lett.*, vol. 34, no. 9, pp. 1003–1006, Oct. 1, 2022.

[7] J. Zhang *et al.*, "Nonlinearity-aware PS-PAM-16 transmission for C-band net-300-Gbit/s/λ short-reach optical interconnects with a single DAC," *Opt. Lett.*, vol. 47, no. 12, pp. 3035–3038, 2022.

[8] H. Yamazaki *et al.*, "Net-400-Gbps PS-PAM transmission using integrated AMUX-MZM," *Opt. Exp.*, vol. 27, no. 18, pp. 25544–25550, 2019.

[9] G. RizzelliMartella, A. Nespola, S. Straullu, F. Forghieri, and R. Gaudino, "Scaling laws for unamplified coherent transmission in next-generation short-reach and access networks," *J. Lightw. Technol.*, vol. 39, no. 18, pp. 5805–5814, Sep. 2021.

[10] J. Zhou and Q. Zhang, "Multiple Tb/s coherent optical transceivers for short reach interconnect," *IEEE J. Sel. Topics Quantum Electron.*, vol. 28, no. 6, Nov./Dec. 2022, Art. no. 8200814.

[11] D. Tauber, "Role of coherent system in the next DCI generation," in *Proc. Opt. Fiber Commun. Conf. (OFC)*, 2022, pp. 1–3.

[12] J. Cheng, C. Xie, M. Tang, and S. Fu, "Power consumption evaluation of ASIC for short-reach optical interconnects," in *Proc. 23rd Opto-Electron. Commun. Conf. (OECC)*, Jul. 2018, pp. 1–2.

[13] J. Cheng, C. Xie, Y. Chen, X. Chen, M. Tang, and S. Fu, "Comparison of coherent and IMDD transceivers for intra datacenter optical interconnects," in *Proc. Opt. Fiber Commun. Conf. (OFC)*, 2019, pp. 1–3.

[14] D. Zhu *et al.*, "Integrated photonics on thin-film lithium niobate," *Adv. Opt. Photon.*, vol. 13, no. 2, pp. 242–352, 2021.

[15] C. Wang *et al.*, "Integrated lithium niobate electro-optic modulators operating at CMOS-compatible voltages," *Nature*, vol. 562, no. 7725, pp. 101–104, Sep. 2018.

[16] L. Wilkinson. *OIF Launches 800G Coherent and Co-Packaging Framework IA Projects, Elects New Board Members/Positions, Officers and Working Group Chairs*. Accessed: Aug. 14, 2022. [Online]. Available: https://www.oiforum.com/technical-work/hot-topics/800g-coherent/

[17] T. Rahman, S. Calabrò, N. Stojanovic, L. Zhang, J. Wei, and C. Xie, "LUT-assisted pre-compensation for 225 Gb/s/λ O-band transmission," in *Proc. Eur. Conf. Opt. Commun. (ECOC)*, 2019, pp. 1–4.

[18] M. Y. S. Sowailem *et al.*, "770-Gb/s PDM-32QAM coherent transmission using InP dual polarization IQ modulator," *IEEE Photon. Technol. Lett.*, vol. 29, no. 5, pp. 442–445, Mar. 1, 2017.

[19] B. Oliveira, A. Lorences-Riesgo, F. Guiomar, M. Medeiros, and P. Monteiro, "Optimizing probabilistic constellation shaping for amplifier-less coherent optical links," *J. Lightw. Technol.*, vol. 39, no. 13, pp. 4318–4330, Jul. 2021.

[20] S. J. Savory, "Digital coherent optical receivers: Algorithms and subsystems," *IEEE J. Sel. Topics Quantum Electron.*, vol. 16, no. 5, pp. 1164–1179, Sep./Oct. 2010.

[21] S. J. Savory, "Digital filters for coherent optical receivers," *Opt. Exp.*, vol. 16, no. 2, pp. 804–817, Jan. 2008.